

good solvent for itself. However, conjugated polymer films are typically prepared by spin coating, which may kinetically trap nonequilibrium ordered collapsed conformations. The presence of such structure could account for the experimentally observed local chain-chain order and anisotropy of such films (36, 37). However, such order could also be produced by parallel packing of chains from different polymer molecules (5). Indeed, both types of chain-chain packing may compete in the highly heterogeneous and variable morphologies of conjugated polymer thin films.

References and Notes

1. R. H. Friend *et al.*, *Nature* **397**, 121 (1999).
2. F. Hide, M. A. Diazgarcia, B. J. Schwartz, A. J. Heeger, *Acc. Chem. Res.* **30**, 430 (1997).
3. T. M. Swager, *Acc. Chem. Res.* **31**, 201 (1998).
4. R. Jakubiak, C. J. Collison, W. C. Wan, L. J. Rothberg, B. R. Hsieh, *J. Phys. Chem. A* **103**, 2394 (1999).
5. T. Q. Nguyen, V. Doan, B. J. Schwartz, *J. Chem. Phys.* **110**, 4068 (1999).
6. H. Sirringhaus *et al.*, *Nature* **401**, 685 (1999).
7. R. Österbacka, C. P. An, X. M. Jiang, Z. V. Vardeny, *Science* **287**, 839 (2000).
8. D. Hu, J. Yu, P. Barbara, *J. Am. Chem. Soc.* **121**, 6936 (1999).
9. D. Hu *et al.*, *Nature* **405**, 1030 (2000).
10. W. E. Moerner and M. Orrit, *Science* **283**, 1670 (1999).
11. S. Weiss, *Science* **283**, 1676 (1999).
12. X. S. Xie and J. K. Trautman, *Annu. Rev. Phys. Chem.* **49**, 441 (1998).
13. T. Basche, W. E. Moerner, M. Orrit, U. P. Wild, *Single Molecule Optical Detection, Imaging, and Spectroscopy* (Verlag Chemie, Munich, 1996).
14. R. Rigler, *J. Biotechnol.* **41**, 177 (1995).
15. D. A. Vandembout *et al.*, *Science* **277**, 1074 (1997).
16. The single-molecule spectra were acquired at ambient temperature using a previously described sample scanning confocal apparatus. Typical conditions for the single-molecule spectra we describe here are excitation spot size = 320 nm, excitation wavelength = 488 nm, and excitation power = 100 nW. The MEH-PPV sample used in the paper was supplied by Uniax Corp.
17. Single-molecule samples were prepared by spin-coating a toluene solution containing 10^{-7} g/ml of MEH-PPV and 10 mg/ml polycarbonate onto a glass substrate. The procedure prepared a film of 500 ± 100 nm thickness. To reduce the O_2 concentration, a freshly spin-coated film was exposed to vacuum (1.0×10^{-5} Pa) for 30 min, and then coated with a 200-nm-thick evaporated Al overlayer in order to seal the film from atmospheric O_2 .
18. H. Bassler and B. Schweitzer, *Acc. Chem. Res.* **32**, 173 (1999).
19. S. Mukamel, S. Tretiak, T. Wagersreiter, V. Chernyak, *Science* **277**, 781 (1997).
20. A. Kohler *et al.*, *Nature* **392**, 903 (1998).
21. H. Meier, U. Stalmach, H. Kolshorn, *Acta Polym.* **48**, 379 (1997).
22. L. Smilowitz, A. Hays, A. J. Heeger, G. Wang, J. E. Bowers, *J. Chem. Phys.* **98**, 6504 (1993).
23. I. D. W. Samuel *et al.*, *Synth. Met.* **84**, 497 (1997).
24. G. Padmanaban and S. Ramakrishnan, *J. Am. Chem. Soc.* **122**, 2244 (2000).
25. A. Y. Grosberg, *Biophysics* **24**, 30 (1979).
26. Y. A. Kuznetsov and E. G. Timoshenko, *J. Chem. Phys.* **111**, 3744 (1999).
27. H. Noguchi and K. Yoshikawa, *J. Chem. Phys.* **109**, 5070 (1998).
28. Y. Q. Zhou, M. Karplus, J. M. Wichert, C. K. Hall, *J. Chem. Phys.* **107**, 10691 (1997).
29. V. Czikkley, H. D. Försterling, H. Kuhn, *Chem. Phys. Lett.* **6**, 11 (1970).
30. G. Bazan *et al.*, *J. Am. Chem. Soc.* **120**, 9188 (1998).
31. C. L. Gettinger, A. J. Heeger, J. M. Drake, D. J. Pine, *J. Chem. Phys.* **101**, 1673 (1994).
32. J. Seth *et al.*, *J. Am. Chem. Soc.* **116**, 10578 (1994).
33. R. Österbacka, M. Wohlgenannt, D. Chinn, Z. V. Vardeny, *Phys. Rev. B* **60**, R11253 (1999).
34. G. D. Hale, S. J. Oldenburg, N. J. Halas, *Phys. Rev. B* **55**, 16069 (1997).
35. M. Yan, L. J. Rothberg, E. W. Kwock, T. M. Miller, *Phys. Rev. Lett.* **75**, 1992 (1995).
36. J. W. Blatchford *et al.*, *Phys. Rev. B* **54**, R3683 (1996).
37. C. Y. Yang, F. Hide, M. A. Diazgarcia, A. J. Heeger, Y. Cao, *Polymer* **39**, 2299 (1998).
38. Supported by grants from NSF and the Robert A. Welch Foundation.

16 February 2000; accepted 28 June 2000

Calcium-Aluminum-Rich Inclusions from Enstatite Chondrites: Indigenous or Foreign?

Yunbin Guan,¹ Gary R. Huss,^{2,3} Glenn J. MacPherson,¹ Gerald J. Wasserburg²

The primary mineral assemblages and initial $^{26}\text{Al}/^{27}\text{Al}$ ratios of rare calcium-aluminum-rich inclusions (CAIs) from enstatite (E) chondrites are similar to those of CAIs from other chondrite classes. CAIs from all chondrite classes formed under oxidizing conditions that are much different from the reducing conditions under which the E chondrites formed. Either CAIs formed at an earlier, more oxidizing epoch in the region where E chondrites ultimately formed, or they formed at a different place in the solar nebula and were transported into the E chondrite formation region.

CAIs are refractory objects that make up <5 volume percent of primitive chondritic meteorites [e.g., (1)]. They were among the first objects formed in the solar nebula ~4.56 billion years ago and therefore bear important physical and chemical information about the earliest stages of solar system evolution. Previous studies demonstrated that CAIs carry excesses of ^{26}Mg compared with the average solar system Mg (2, 3). These ^{26}Mg excesses correlate with the Al/Mg ratios of the host minerals within individual CAIs and therefore are due to in situ decay of the short-lived radionuclide ^{26}Al [half-life ($t_{1/2}$) ~730,000 years] that was present in the inclusions when they formed. Voluminous data for CAIs in carbonaceous (C) chondrites (4) establish a canonical initial abundance ratio, ($^{26}\text{Al}/^{27}\text{Al}$)₀, for the early solar system of $\sim 5 \times 10^{-5}$. CAIs in ordinary (O) chondrites share this same initial ratio (5). However, some rare CAIs from C and O chondrites formed with little or no ^{26}Al . Either those inclusions formed several million years after most CAIs (i.e., after ^{26}Al had largely decayed), or ^{26}Al was heterogeneously distributed in the early solar system.

CAIs from C and O chondrites share sim-

ilar mineral assemblages and distinctive oxygen isotopic features, raising the possibility that CAIs might have formed in a single restricted region of the solar nebula (6). A way to test this interesting possibility is to study CAIs from E chondrites. E chondrites have distinctive mineral assemblages that could only have formed under reducing conditions (7), and they may have formed in a different region of the solar nebula than C and O chondrites. If CAIs in E chondrites share this distinctive reduced mineral assemblage and yet share the isotopic characteristics of CAIs in C and O chondrites, this would indicate that refractory objects formed in many different nebular locales from broadly similar isotopic reservoirs. Such a result would support the idea that ^{26}Al was widely distributed in the early solar nebula. Alternatively, if CAIs in E chondrites are mineralogically similar to CAIs in C and O chondrites and lack the extremely reduced phases of the host E chondrites, this would imply that all CAIs formed under similar conditions, perhaps in a single region from which they were broadly distributed.

Here, we report the results of a systematic search for and Mg-isotopic analysis of CAIs in 26 polished thin sections of 14 unequilibrated E chondrites. Seventy-two CAIs >10 μm across and eight isolated hibonite and spinel mineral fragments were identified by x-ray area mapping of the thin sections (Table 1). These inclusions were studied by scan-

¹Department of Mineral Sciences, National Museum of Natural History, Smithsonian Institution, Washington, DC 20560-0119, USA. ²Lunatic Asylum, Division of Geological and Planetary Sciences 170-25, California Institute of Technology, Pasadena, CA 91125, USA. ³Department of Geology and Center for Meteorite Studies, Arizona State University, Tempe, AZ 85287-1404, USA.

REPORTS

ning electron microscopy (SEM); mineral compositions were determined by electron microprobe and SEM (8). CAIs containing mineral phases with high Al/Mg ratios were chosen for Mg- and Ti-isotopic studies. Isotopic measurements were made with PANURGE, a modified CAMECA ims-3f ion microprobe at Caltech, with standard techniques (9, 10).

The abundance of CAIs varies greatly from meteorite to meteorite. More than half of the E chondrites we searched are virtually devoid of CAIs, whereas EET87746 and Sahara 97072 contain numerous inclusions (Table 1). All CAIs and Al-rich mineral fragments found in this study are <120 μm in diameter, and the majority are <50 μm, consistent with previous observations (11). CAIs in E chondrites are thus smaller than their counterparts in C and O chondrites, but their primary mineral assemblages are similar (1, 12). Most inclusions consist of spinel and hibonite or spinel, pyroxene, and plagioclase, with perovskite and Fe-Ni metal as common accessories (13). One melilite-bearing inclusion was found, and several inclusions exhibit Wark-Lovering rims (14). All inclusions show significant secondary processing. The population of E chondrite CAIs thus differs from those in other chondrite classes mainly in terms of relative abundances of different CAI types and the sizes of the inclusions (1, 15).

The back-scattered electron photomicrographs (Fig. 1) illustrate the diversity of CAIs in E chondrites. Inclusion E4631-1 (16) from EET87746 is a melilite-bearing CAI (Fig. 1A). It consists of densely intergrown spinel and melilite with small (<5 μm), enclosed grains of perovskite (CaTiO₃) and the rare mineral geikielite (MgTiO₃). The melilite is Al-rich (Åk₃₋₁₈), with Na₂O and FeO <0.5 weight % (wt%) and TiO₂ <0.2 wt%. The edges of melilite and spinel grains in E4631-1 are corroded in appearance and surrounded by a fine-grained mixture of Na-rich secondary phases. Hibonite-bearing CAIs are relatively common among CAIs from E chondrites. Inclusion E4640-1 from EET87746 (Fig. 1B) is an oblong CAI consisting of intergrown euhedral hibonite blades (<5 × 10 μm), spinel, and abundant interstitial troilite (~0.9 wt% Cr, ~1.8 wt% Ti, and <0.1 wt% Mn). A ~2- to 4-μm-thick Wark-Lovering rim of aluminous diopside (1.5 to 6.5 wt% Al₂O₃, 2 to 4.2 wt% FeO) surrounds most of the CAI. Separating the rim from the spinel-hibonite interior is a <5-μm-thick porous zone consisting of fine-grained anhydrous Mg-Al silicate and sodalite. The most common type of CAI in E chondrites (51 of 72 in this study) consists mainly of spinel (e.g., S721-12; Fig. 1C). Pyroxene is a common additional phase, along with perovskite, troilite, and geikielite. These inclusions are diverse in their size, morphology, texture, secondary alteration, and mineral compo-

nents. Some have well-defined Wark-Lovering rims and others do not. Finally, inclusion E4631-3 from EET87746 is a ~40-μm-diameter microspherule consisting of two euhedral hibonite grains enclosed in pyroxene, with tiny crystals of perovskite enclosed in the hibonite (Fig. 1D). Similar hibonite-bearing microspherules have been found in C chondrites (15, 17, 18).

Before the current study, no evidence of live ²⁶Al had been detected in CAIs from E chondrites, and Ti (and Ca) isotopes had been measured in only one hibonite-bearing inclusion from Qingzhen (19). In this study, we measured Mg-isotopic compositions in 11 hibonite-bearing inclusions or fragments from

ALHA77295, EET87746, and Sahara 97072. Seven contain resolved excesses of radiogenic ²⁶Mg (≡²⁶Mg*), and four others do not (Table 2). The relatively large inclusion E4640-1 has resolved ²⁶Mg* excesses that correlate with Al/Mg ratios and give an inferred (²⁶Al/²⁷Al)₀ of (3.3 ± 1.1) × 10⁻⁵ (Fig. 2A). Because many of the CAIs are <50 μm across and their mineral phases are <15 μm across, only one or two spots could be measured on each CAI. Nonetheless, two-point (e.g., Fig. 2B) and model isochrons (which assume normal ²⁶Mg/²⁴Mg for the low-Al phase) yield (²⁶Al/²⁷Al)₀ ratios ~5 × 10⁻⁵, the canonical value obtained from many CAIs in C and O chondrites (2-4).

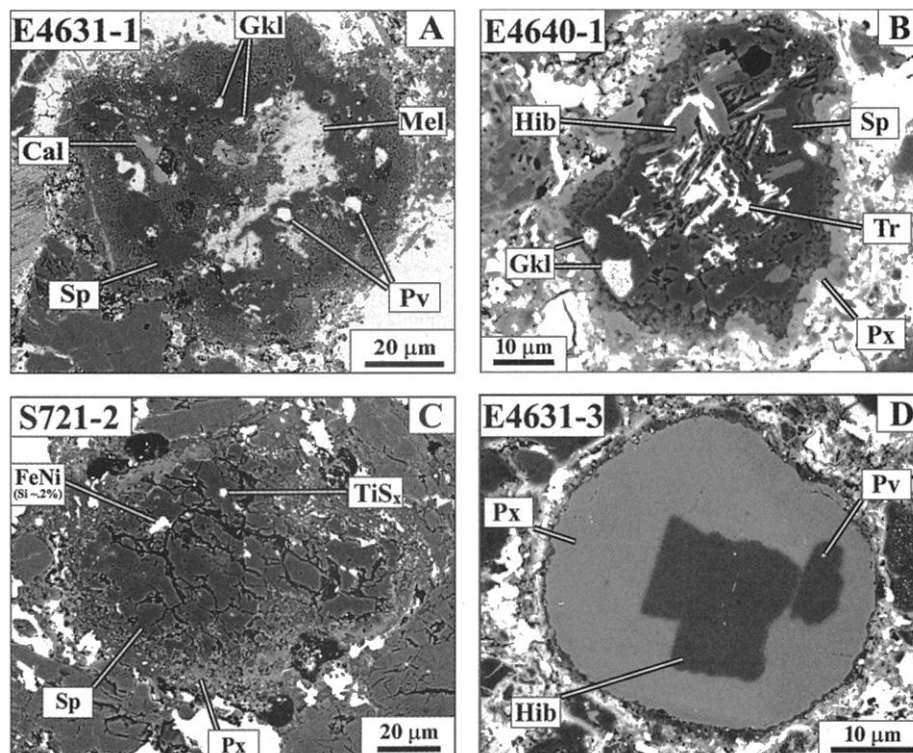


Fig. 1. Back-scattered electron images of CAIs in E chondrites. (A) A melilite-bearing CAI in which melilite (Mel) and spinel (Sp) are altered to fine-grained Al-Mg silicate and sodalite. Gkl, geikielite; Pv, perovskite; Cal, calcite. (B) A hibonite (Hib)-spinel inclusion with an incomplete Wark-Lovering rim. Tr, troilite. (C) A spinel-pyroxene (Px) CAI containing Fe-Ni metal and a titanium sulfide (TiS_x). (D) A hibonite-pyroxene (Px) microspherule.

Table 1. CAIs and hibonite or spinel fragments in E chondrites. Mel, melilite; Hib, hibonite; Sp, spinel; Px, pyroxene; Pl, plagioclase; Frag, Sp or Hib fragments.

Sample	No. of thin sections	Mel-Sp	Hib-Px	Hib-Sp	Sp-Px-Pl	Frag	Sum
ALHA77295 (EH3)	3	0	0	3	10	2	15
EET87746 (EH3)	3	1	1	10	14	1	27
MAC88136 (EL3)	2	0	0	0	1	1	2
PCA91020 (EL3)	2	0	0	0	4	0	4
Qingzhen (EH3)	6	0	0	2	6	1	9
Sahara 97072 (EH3)	2	0	0	4	16	3	23
Total	26*	1	1	19	51	8	80

*One thin section from each of the following samples was searched, but no CAI was found: Abee (EH4), Adhi Krot (EH4), GRO95517 (EH3), Indarch (EH4), Kota Kota (EH3), Parsa (EH3), PCA91085 (EH3), and PCA91238 (EH3).

REPORTS

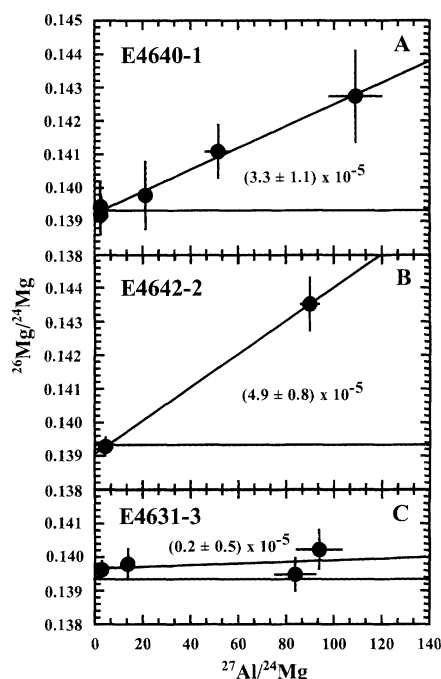


Fig. 2. Mg-Al isotopic systematics for three CAIs from E chondrites. (A) and (B) are hibonite-spinel inclusions. (C) is the hibonite-pyroxene microspherule that shows no resolvable $^{26}\text{Mg}^*$ excess. The $(^{26}\text{Al}/^{27}\text{Al})_0$ ratios are listed on the plot for each inclusion.

Hibonite shows little or no sign of mass fractionation of Mg isotopes, but spinel in some cases is slightly enriched in heavy Mg isotopes [$F_{\text{Mg}} \sim 5.0$ per mil (‰)]. The hibonite-bearing microspherule, E4631-3, shows no resolvable $^{26}\text{Mg}^*$ [$(^{26}\text{Al}/^{27}\text{Al})_0 \leq 0.7 \times 10^{-5}$] (Fig. 2C) and no nonlinear isotopic effects in Ti (errors $\pm 4\%$). Neither element is mass fractionated. Ti-isotopic compositions were measured in two additional inclusions, E4640-1 and A9528-2, and no nonlinear anomalies or mass fractionation effects were observed.

The characteristic minerals of E chondrites constitute an unusual assemblage of reduced silicates, sulfides, carbides, and nitrides that represents conditions so reducing that normally lithophile elements such as Ca, Cr, Ti, and Mn occur in sulfides (7, 20). Also, substantial metallic Si is dissolved in the Fe-Ni metal. Interpreted in terms of equilibrium condensation, the E chondrite mineralogy implies a nebular C/O ratio >1 (20), whereas the assemblages from C and O chondrites indicate a C/O ratio <1 .

In contrast, the original mineral assemblages of CAIs in E chondrites are not consistent with such highly reducing conditions. The minerals that crystallized when the inclusions first formed include hibonite, melilite, spinel, perovskite, pyroxene, and Fe-Ni metal. Mineral compositions are similar to those in CAIs from C and O chondrites (13). The

Table 2. Al-Mg isotopic data for CAIs from E chondrites. Mg isotopes are typically reported as Δ values, the deviation in ‰ relative to a standard composition: $\Delta^{26}\text{Mg} = [({}^{26}\text{Mg}/{}^{24}\text{Mg})_{\text{sample}} / ({}^{26}\text{Mg}/{}^{24}\text{Mg})_{\text{standard}} - 1] \times 1000$, where $m = 25, 26$.

Mineral	F(Mg) [†]	$\delta^{26}\text{Mg}^*$	$^{27}\text{Al}/^{24}\text{Mg}$
<i>E4640-1</i> ($^{26}\text{Al}/^{27}\text{Al})_0 = (3.3 \pm 1.1) \times 10^{-5}$			
Hibonite	-4.6 ± 4.4	22.8 ± 9.8	109 ± 11
Hibonite	-0.4 ± 3.3	1.7 ± 7.2	21.2 ± 2.1
Hibonite	1.0 ± 2.5	11.0 ± 5.6	51.7 ± 5.2
Spinel	7.0 ± 2.5	-0.8 ± 5.3	2.4 ± 0.2
Spinel	3.8 ± 1.9	-2.5 ± 4.2	2.5 ± 0.3
Spinel	5.0 ± 1.3	-1.5 ± 2.6	2.7 ± 0.3
<i>E4631-3</i> ($^{26}\text{Al}/^{27}\text{Al})_0 \leq 0.7 \times 10^{-5}$			
Hibonite	-0.9 ± 1.9	4.8 ± 4.1	93.9 ± 9.4
Hibonite	0.4 ± 1.6	-0.5 ± 3.5	83.9 ± 8.4
Pyroxene	0.2 ± 1.2	0.5 ± 1.9	2.8 ± 0.3
Pyroxene	-5.3 ± 1.7	1.7 ± 3.2	13.7 ± 1.4
<i>E4642-2</i> ($^{26}\text{Al}/^{27}\text{Al})_0 = (5.0 \pm 0.8) \times 10^{-5}$			
Hibonite	-3.9 ± 2.5	30.1 ± 5.6	89.9 ± 3.7
Spinel	3.8 ± 1.0	-0.3 ± 2.0	4.5 ± 0.3
<i>E4642-4</i> ($^{26}\text{Al}/^{27}\text{Al})_0 \leq 1.0 \times 10^{-5}$			
Hibonite	-3.8 ± 2.2	-0.2 ± 4.9	76.1 ± 2.9
Spinel	5.6 ± 1.5	-1.4 ± 3.2	4.7 ± 0.3
<i>E4642-8</i> ($^{26}\text{Al}/^{27}\text{Al})_0 = (5.4 \pm 1.7) \times 10^{-5}$			
Hibonite	1.4 ± 1.7	10.1 ± 3.8	31.3 ± 1.1
Spinel	3.2 ± 1.4	-0.7 ± 2.6	3.2 ± 0.3
<i>E4642-12</i> ($^{26}\text{Al}/^{27}\text{Al})_0 = (3.8 \pm 0.9) \times 10^{-5}$			
Hibonite	0.6 ± 11.7	15.7 ± 24.7	114 ± 12
Hibonite	-3.6 ± 2.3	25.0 ± 5.2	81.2 ± 2.6
<i>E4642-15</i> ($^{26}\text{Al}/^{27}\text{Al})_0 = (4.0 \pm 1.1) \times 10^{-5}$			
Hibonite	-3.7 ± 4.0	19.4 ± 8.9	65.6 ± 3.9
Hibonite	-4.2 ± 2.8	20.9 ± 6.3	75.0 ± 3.1
<i>S721-5</i> ($^{26}\text{Al}/^{27}\text{Al})_0 = (4.4 \pm 1.0) \times 10^{-5}$			
Hibonite	-3.2 ± 2.5	24.7 ± 5.4	78.6 ± 2.4
<i>S722-9</i> ($^{26}\text{Al}/^{27}\text{Al})_0 = (3.9 \pm 1.5) \times 10^{-5}$			
Hibonite	-0.7 ± 1.4	7.9 ± 3.0	28.2 ± 1.4
<i>S722-13</i> ($^{26}\text{Al}/^{27}\text{Al})_0 \leq 1.5 \times 10^{-5}$			
Hibonite	-1.3 ± 2.7	-0.5 ± 6.2	51.8 ± 3.7
<i>A9528-2</i> ($^{26}\text{Al}/^{27}\text{Al})_0 \leq 2.5 \times 10^{-6}$			
Hibonite	0.6 ± 4.6	-13.0 ± 10.1	135 ± 14
Spinel	0.5 ± 1.8	1.0 ± 3.7	2.7 ± 0.3

[†]The sample mass fractionation: $F(\text{Mg}) = (\Delta^{25}\text{Mg})_{\text{sample}} - (\Delta^{25}\text{Mg})_{\text{standard}}$. *Excesses in ^{26}Mg are given by $\delta^{26}\text{Mg} = \Delta^{26}\text{Mg} - 2 \times \Delta^{25}\text{Mg}$. All errors are 2σ .

Fe-Ni metal in S721-2 (Fig. 1C) contains <0.2 wt % Si, whereas metal in the host meteorite contains ~ 2.5 wt % Si. None of the CAIs contain the reduced phases, oldhamite (CaS) or osbornite (TiN). Many CAIs from E chondrites experienced a secondary event that deposited rims of aluminous diopside, fine-grained aluminosilicates, and sodalite (e.g., E4640-1) and sometimes resulted in partial replacement of primary minerals such as melilite by fine-grained, Na-rich aluminosilicates (e.g., E4631-1). This second event also occurred under relatively oxidizing conditions, as shown by the high FeO content of rim pyroxenes, and is also recorded in CAIs from C and O chondrites. We conclude that the CAIs in E chondrites formed under conditions more oxidizing than those of the host chondrites and similar to those of CAIs in C and O chondrites.

Al-Mg isotopic systematics of E chondrite CAIs are also similar to those of C and O chondrites. The majority of CAIs reported

here formed with $(^{26}\text{Al}/^{27}\text{Al})_0 \approx 4$ to 5×10^{-5} (Table 2), like CAIs from C and O chondrites (4). But, just as in C and O chondrites, some CAIs lack $^{26}\text{Mg}^*$.

Although similar in primary minerals and Al-Mg systematics to CAIs from C and O chondrites, CAIs from E chondrites also carry a very late-stage (post-rimming) overprint of highly reduced minerals not seen in CAIs from other types of chondrites. Troilite containing 2 to 7 wt% Ti occurs interstitially, along cracks, and within voids in several inclusions (e.g., E4640-1). In contrast, the troilite in CAIs from C and O chondrites is typically Ti-poor [Ti $\ll 0.1$ wt% (12)]. We also observed a Ti sulfide in two CAIs, although the crystals are too small to determine the stoichiometry. The Mg-Ti oxide, geikielite, is an accessory phase in several of the E chondrite CAIs. In some cases, geikielite rims and appears to be replacing perovskite (Fig. 3A). The geikielite in turn is commonly rimmed by Ti-rich troilite (Fig. 3B), suggest-

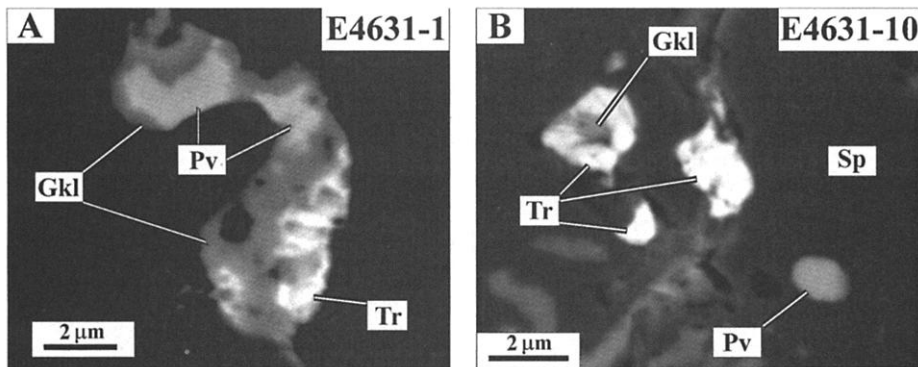


Fig. 3. Back-scattered electron images showing the relations between perovskite (Pv), geikielite (Gkl), and Ti-rich troilite (Tr). (A) Geikielite rims, and appears to replace, perovskite in E4631-1. (B) Geikielite is rimmed by Ti-enriched troilite along the cracks in E4631-10, whereas a perovskite grain is enclosed inside spinel (Sp).

ing that the order of formation was perovskite, then geikielite, and then troilite. Although geikielite has been observed in a CAI from the C chondrite Ningqiang (21), it is typically not found in CAIs outside of E chondrites. We cannot determine unambiguously whether the geikielite formed under oxidizing or reducing conditions, but the relatively common occurrence in E chondrites implies that geikielite formation is favored by reducing conditions. The replacement of geikielite by Ti-rich troilite requires reducing conditions. Therefore, we infer that the late-stage conditions under which the sulfides in these CAIs formed were distinctly more reducing than those under which the inclusions originally formed.

Chondrites are aggregates of diverse materials, some of which (e.g., presolar grains) clearly formed outside of the regions where the chondrites accumulated. The question of interest here is, are the CAIs likewise “foreign” or did they form by some special process in the same general region where the chondrites accreted? The special properties of E chondrites provide clues to the answer. Their highly reduced mineral assemblage requires that E chondrites formed under conditions far more reducing than those experienced by other chondrites. Yet, the primary minerals and mineral chemistry of E chondrite CAIs suggest formation under relatively more oxidizing conditions than their host meteorites.

Two models might explain these seemingly contradictory observations. The first possibility is that all CAIs formed by a special process that occurred in many regions of the solar nebula, including those where the diverse chondrite types ultimately accreted. In this model, the $(^{26}\text{Al}/^{27}\text{Al})_0$ ratios of $\sim 5 \times 10^{-5}$ observed in the E chondrite CAIs reflect the local isotopic composition of material in the E chondrite formation region. This model requires that the E chondrite accretion region was relatively oxidizing at the time of CAI forma-

tion and then evolved through time to a much more reduced state. Circumstantial support for such a model comes from the presence in some unequilibrated E chondrites of chondrules that contain FeO-bearing silicates in their cores but reduced phases in their rims (22, 23). However, mineralogical properties and Al-Mg systematics suggest that CAIs from C, O, and E chondrites all formed under similar conditions throughout the various chondrite accretion regions. In this model, the CAIs (and the FeO-bearing chondrules?) are foreign to the formation region of the E chondrites. For example, Shu *et al.* (24) suggested that CAIs formed near the sun and bipolar outflow then carried them out into the wider nebula. An important implication of this type of model is that the inferred $(^{26}\text{Al}/^{27}\text{Al})_0$ ratios of CAIs from C, O, and E chondrites may not reflect the ratios where the chondrites accreted. In both models, the characteristic reduced E chondrite minerals were superimposed on earlier more oxidized assemblages by some late-stage process.

References and Notes

1. G. J. MacPherson, D. A. Wark, J. T. Armstrong, in *Meteorites and the Early Solar System*, J. F. Kerridge and M. S. Matthews, Eds. (Univ. of Arizona Press, Tucson, AZ, 1988), pp. 746–807.
2. T. Lee, D. A. Papanastassiou, G. J. Wasserburg, *Geophys. Res. Lett.* **3**, 109 (1976).
3. ———, *Astrophys. J.* **211**, L107 (1977).
4. G. J. MacPherson, A. M. Davis, E. K. Zinner, *Meteoritics* **30**, 365 (1995).
5. S. S. Russell, G. Srinivasan, G. R. Huss, G. J. Wasserburg, G. J. MacPherson, *Science* **273**, 757 (1996).
6. K. D. McKeegan, L. A. Leshin, S. S. Russell, G. J. MacPherson, *Science* **280**, 414 (1998).
7. K. Keil, *Meteoritics* **24**, 195 (1989).
8. X-ray mapping was done with a JEOL-840A scanning

electron microscope and a KeveX energy-dispersive detector system. Major-element chemistries of most minerals were determined by wavelength-dispersive techniques with a JEOL-JXA 8900R electron microprobe operated at 15 kV with a probe current of 20 nA. Fine-grained (<5 μm) mineral phases were analyzed by standardized quantitative energy-dispersive x-ray analysis, with the SEM system operating at 10-kV accelerating voltage and 1-nA beam current.

9. J. C. Huneke, J. T. Armstrong, G. J. Wasserburg, *Geochim. Cosmochim. Acta* **47**, 1635 (1983).
10. A. J. Fahey, J. N. Goswami, K. D. McKeegan, E. K. Zinner, *Geochim. Cosmochim. Acta* **51**, 329 (1987).
11. A. Bischoff, K. Keil, D. Stöffler, *Chem. Erde* **44**, 97 (1985).
12. A. J. Brearley and R. H. Jones, in vol. 36 of *Reviews in Mineralogy*, J. J. Papike, Ed. (Mineralogical Society of America, Washington, DC, 1998), chap. 3.
13. Hibonites from the CAIs display ranges in TiO₂ (<0.1 to 5.75 wt %) and MgO (0.31 to 4.75 wt %) contents that are similar to hibonites in spinel-hibonite inclusions from Murchison and Mighei (CM2). Calculated as atoms per formula unit, there is an inverse correlation of Mg + Fe + Ti + Si with Al + V + Cr, consistent with the coupled substitution $R^{2+} + R^{4+} \leftrightarrow 2R^{3+}$ and suggesting that Ti is quadrivalent in these hibonites. Spinel (MgAl₂O₄) contains little FeO (<0.8 wt%) and Cr₂O₃ (<0.5 wt%). Perovskite is pure CaTiO₃. Pyroxenes show large compositional variations. Most have TiO₂ concentrations <4 wt%, except for those in CAI A9528-3, which contain TiO₂ up to 16 wt%. Pyroxene inside some rimmed inclusions has relatively higher concentrations of TiO₂ (up to 8.2 wt%) and Al₂O₃ (up to 27 wt%) than those on the rim itself (TiO₂ < 1.2 wt%; Al₂O₃ < 13 wt%). This feature is observed in rimmed CAIs from C and O chondrites. The composition of pyroxene in the hibonite-bearing microspherule falls in the solid solution between diopside (CaMgSi₂O₆) and Ca-Tschermak's molecule (CaAl₂SiO₆). It is distinguished from pyroxenes in other CAIs by higher Al₂O₃ (24 to 39 wt%) and lower SiO₂ (<40 wt%). Its TiO₂ abundance ranges from 0.5 to 2.8 wt%. There is a clear chemical zoning in which SiO₂ and MgO are strongly correlated with each other and are anticorrelated with Al₂O₃ and TiO₂. Similar chemical characteristics were also observed in pyroxene of microspherules from C chondrites.
14. D. A. Wark and J. F. Lovering, *Proc. Lunar. Planet. Sci. Conf.* **8**, 95 (1977).
15. S. S. Russell *et al.*, *Geochim. Cosmochim. Acta* **62**, 689 (1998).
16. CAIs are labeled with a shorthand notation as follows: The first three characters represent the first letter and last two numbers from the meteorite name, the next two numbers are the individual thin section number, and the last number is the specific CAI identification number; e.g., E4631-1 is CAI#1 from EET87746 PTS#31, S721-12 is CAI#12 from Sahara 97072 PTS#1, and A9528-2 is CAI#2 from ALHA77295 PTS#28.
17. T. R. Ireland, A. J. Fahey, E. K. Zinner, *Geochim. Cosmochim. Acta* **55**, 367 (1991).
18. S. B. Simon, A. M. Davis, L. Grossman, E. K. Zinner, *Meteorit. Planet. Sci.* **33**, 411 (1998).
19. A. J. Fahey, thesis, Washington University, St. Louis, MO (1988).
20. J. W. Larimer and M. Bartholomay, *Geochim. Cosmochim. Acta* **43**, 1455 (1979).
21. Y. Lin and M. Kimura, *Lunar Planet. Sci.* **XVII**, 755 (1996).
22. D. Lusby, E. R. D. Scott, K. Keil, *Proc. Lunar Planet. Sci. Conf. 17th, J. Geophys. Res.* **92** (no. B4), E679 (1987).
23. J. N. Grossman, G. J. MacPherson, G. Crozaz, *Meteoritics* **28**, 358 (1993).
24. F. H. Shu, H. Shang, T. Lee, *Science* **271**, 1545 (1996).
25. Supported by NASA grants NAG5-7396 (G.J.M.), NAG5-4083 (G.J.W.), and NAG5-8158 (G.R.H.). We thank the Antarctic Meteorite Working Group and NASA Johnson Space Center for providing the Antarctic meteorite thin sections. Caltech Division Contribution 8652 (1044).

19 April 2000; accepted 15 June 2000